
**STATE RESEARCH CENTER OF RUSSIA**

**INSTITUTE FOR HIGH ENERGY PHYSICS**

IHEP 97-83

V.Ammosov, V.Korablev*, R.Santonico[1]

# INDUCED CHARGES AND VOLTAGE SIGNALS IN RESISTIVE PLATE CHAMBERS

Submitted to *NIM*

[1]University of Rome "Tor Vergata", Italy
*Correspondent author. E–mail: korablev@mx.ihep.su

Protvino 1997

UDK 537.613 M–24

**Abstract**

Ammosov V., Korablev V., Santonico R. Induced charges and voltage signals in resistive plate chambers: IHEP Preprint 97-83. – Protvino, 1997. – p. 26, figs. 13, tables 2, refs.: 4.

Charge density distributions and voltage signals, which are induced in a resistive plate chamber (RPC) with an avalanche fast component, were simulated for different RPC design. The simulation data have allowed one to understand what factors have more essential influence on the value of the induced charge and voltage signal in a RPC.

**Аннотация**

Аммосов В., Кораблев В., Сантонико Р. Наведенные заряды и импульсы напряжения в резистивных плоскопараллельных камерах: Препринт ИФВЭ 97-83. – Протвино, 1997. – 26 с., 13 рис., 2 табл., библиогр.: 4.

Моделирование плотностей зарядов и импульсов напряжения, наведенных быстрой компонентой лавинного процесса в резистивной плоскопараллельной камере (РПК), произведено для различных вариантов РПК. Результаты моделирования позволили понять, какие факторы имеют наибольшее влияние на величину наведенного заряда и импульса напряжения в РПК.

# Introduction

For calculations we used the surface charges method (SCM) that is described in [1].

In Section 1 we derive the analytical expressions for the charges, which are induced in metallic planes by the point charge and charged dipole.

In Section 2 we confirm the correctness of applied SCM calculation procedure by the direct comparison of calculated results with analytical predictions.

In Section 3 we consider the field distortion in an avalanche region and estimate the maximal dead region for 2 mm gap RPC, working in an avalanche mode.

In Section 4 we consider the influence of broken foil coating and external ground planes on the value of induced charge for the particle, that goes through the gap between read-out strips.

In Section 5 we study the dependence of induced charge value in the pick-up and neighbouring read-out strips on an avalanche position for unbroken and broken foil coatings and different strip widths.

In Section 6 we consider the voltage signal dependence on electrode thickness, permittivity and the distance between ground and strip plane.

The basic RPC scheme under consideration has transverse dimension $50\times50$ cm$^2$ and 2 mm gap. In sections $2\div6$ we work with 50 pC avalanche. This value in 2 mm gap RPC is close to streamer–avalanche boundary ($\alpha g \sim 20$) for the exponential discharge process $Q_{gap}=q_e e^{\alpha g}$ ($q_e$ is the electron charge, $\alpha$ is the Tounsend coefficient, g is the gas gap value).

# 1. Charges induced by point charge and charged dipole

## 1.1. Point charge near metallic plane

Let the point charge $Q_0$ be placed at a distance h from the infinite metallic foil plane (Fig.1a), which is under the ground potential. Let r be the distance along the plane surface from the centre of symmetry of the picture up to the plane point, where we are interested in the field value. In such terms the spacial distance R from the charge $Q_0$ up to plane point is determined $R=\sqrt{r^2+h^2}$. Charge $Q_0$ induces in the metallic foil a

definite charge density distribution $\sigma(r)$ to provide zero field in the opposite (relative to charge position) side of the plane. For this side we can write down the condition of zero normal field component for an arbitrary plane point as:

$$\frac{\sigma(r)}{2\varepsilon_0} + \frac{Q_0}{4\pi\varepsilon_0} \cdot \frac{h}{(\sqrt{r^2+h^2})^3} = 0 \tag{1}$$

and solve this equation relative to unknown function $\sigma(r)$

$$\sigma(r) = -\frac{Q_0}{2\pi} \cdot \frac{h}{(\sqrt{r^2+h^2})^3}. \tag{2}$$

Integral over a whole plane surface

$$\int_0^\infty \sigma(r) 2\pi r dr = -Q_0 \tag{3}$$

gives the total induced charge, which is equal, in absolute value, to initiating charge $Q_0$ and has the opposite sign.

### 1.2. Charged dipole near metallic plane

Using the superposition principle for the set of point charges $Q_i$ with coordinates $x_i$,$y_i$ and distances $h_i$ up to the metallic, plane we expect the following induced charge density distribution:

$$\sigma(x,y) = -\frac{1}{2\pi} \cdot \sum_i \frac{Q_i \cdot h_i}{(\sqrt{(x-x_i)^2+(y-y_i)^2+h_i^2})^3}. \tag{4}$$

For the charged dipole (Fig.1a) with transverse orientation of the electric dipole moment relative to metallic plane, we have the following induced charge density distribution:

$$\sigma(r) = \frac{Q_0}{2\pi} \cdot \left(\frac{h_-}{(\sqrt{r^2+h_-^2})^3} - \frac{h_+}{(\sqrt{r^2+h_+^2})^3}\right). \tag{5}$$

Here $h_-$ and $h_+$ are the distances of the negative and positive charges up to the plane ($h_- < h_+$) respectively, $Q_0$ is the value of dipole charge.

When dipole arm $\ell = h_+ - h_-$ is much less in comparison with a distance from the dipole centre up to the plane $h = 0.5 \cdot (h_+ + h_-)$, formula (5) transforms into expression:

$$\sigma(r) = \frac{\ell \cdot Q_0}{2\pi} \cdot \frac{2h^2 - r^2}{(\sqrt{r^2+h^2})^5}. \tag{6}$$

An integrated induced charge value both for expression (5) and for (6) is equal to zero.

### 1.3. Point charge between two metallic planes

For the point charge $Q_0$ between two infinite metallic planes (Fig.1b), the induced charges $Q_1$ and $Q_2$ in the planes can be estimated by the following way. We require the

potentials in points A and B be equal to zero and solve the task under condition H≫h to replace the smeared induced charges in the planes by equivalent point charges $Q_1$ and $Q_2$.

Then

$$P_A = \frac{Q_1}{H} + \frac{Q_2}{H+h} + \frac{Q_0}{H+h_1} = 0, \tag{7}$$
$$P_B = \frac{Q_1}{H+h} + \frac{Q_2}{H} + \frac{Q_0}{H+h_2} = 0,$$

or

$$Q_1 + \frac{H}{H+h} \cdot Q_2 = -\frac{H}{H+h_1} \cdot Q_0, \tag{8}$$
$$\frac{H}{H+h} \cdot Q_1 + Q_2 = -\frac{H}{H+h_2} \cdot Q_0.$$

From the condition H≫h we have $\frac{H}{H+h} \approx 1 - \frac{h}{H}$ and the final system of linear equations

$$Q_1 + (1 - \frac{h}{H}) \cdot Q_2 = -(1 - \frac{h_1}{H}) \cdot Q_0, \tag{9}$$
$$(1 - \frac{h}{H}) \cdot Q_1 + Q_2 = -(1 - \frac{h_2}{H}) \cdot Q_0$$

has the solution

$$Q_1 = -\frac{h_2}{h} \cdot Q_0, \tag{10}$$
$$Q_2 = -\frac{h_1}{h} \cdot Q_0.$$

We see that the total induced charge in both the planes is again equal, in an absolute value, to initiating charge $Q_0$ and has the opposite sign.

### 1.4. Charged dipole between two metallic planes

To estimate the value of induced charge $Q_{ind}$(Fig.1c) from the charged dipole, which is placed between two metallic planes, we can using the same procedure as in Section 1.3. We again require for the potential at a large distance (R≫h) be equal to zero.

$$P = \frac{1}{4\pi\varepsilon_0} \cdot (\frac{(\vec{M}_{ind} \cdot \vec{R}_1)}{R_1^3} + \frac{(\vec{M}_0 \cdot \vec{R}_2)}{R_2^3}) = \frac{1}{4\pi\varepsilon_0} \cdot (M_{ind} \cdot \frac{cos\varphi_1}{R_1^2} - M_0 \cdot \frac{cos\varphi_2}{R_2^2}) = 0. \tag{11}$$

Here $M_{ind}$=h·$Q_{ind}$ and $M_0$=$\ell$·$Q_0$ are the electric dipole moments.

It is clear that for a large distance R an angle $\varphi_1$ is close to $\varphi_2$ (we label this angle as $\varphi$) and denominators $R_1^n$ in expression (11) are close to denominators $R_2^n$. And we can write

$$P = \frac{1}{4\pi\varepsilon_0} \cdot (M_{ind} - M_0) \cdot \frac{cos\varphi}{R^2} = 0. \tag{12}$$

The above equation is satisfied, when

$$Q_{ind} = \frac{\ell}{h} \cdot Q_0. \tag{13}$$

If the dipole is located in gas gap (g), which is separated from metallic planes by dielectric plates with permittivity ($\varepsilon$) and thickness (t), then instead of vacuum distance h we take an equivalent dielectric distance h′=g+2·$\frac{t}{\varepsilon}$ and the value of induced charge now is:

$$Q_{ind} = \frac{\ell}{h'} \cdot Q_0 = \frac{\ell}{g + 2\frac{t}{\varepsilon}} \cdot Q_0. \tag{14}$$

This formula can be derived in other ways (see, for example [2]).

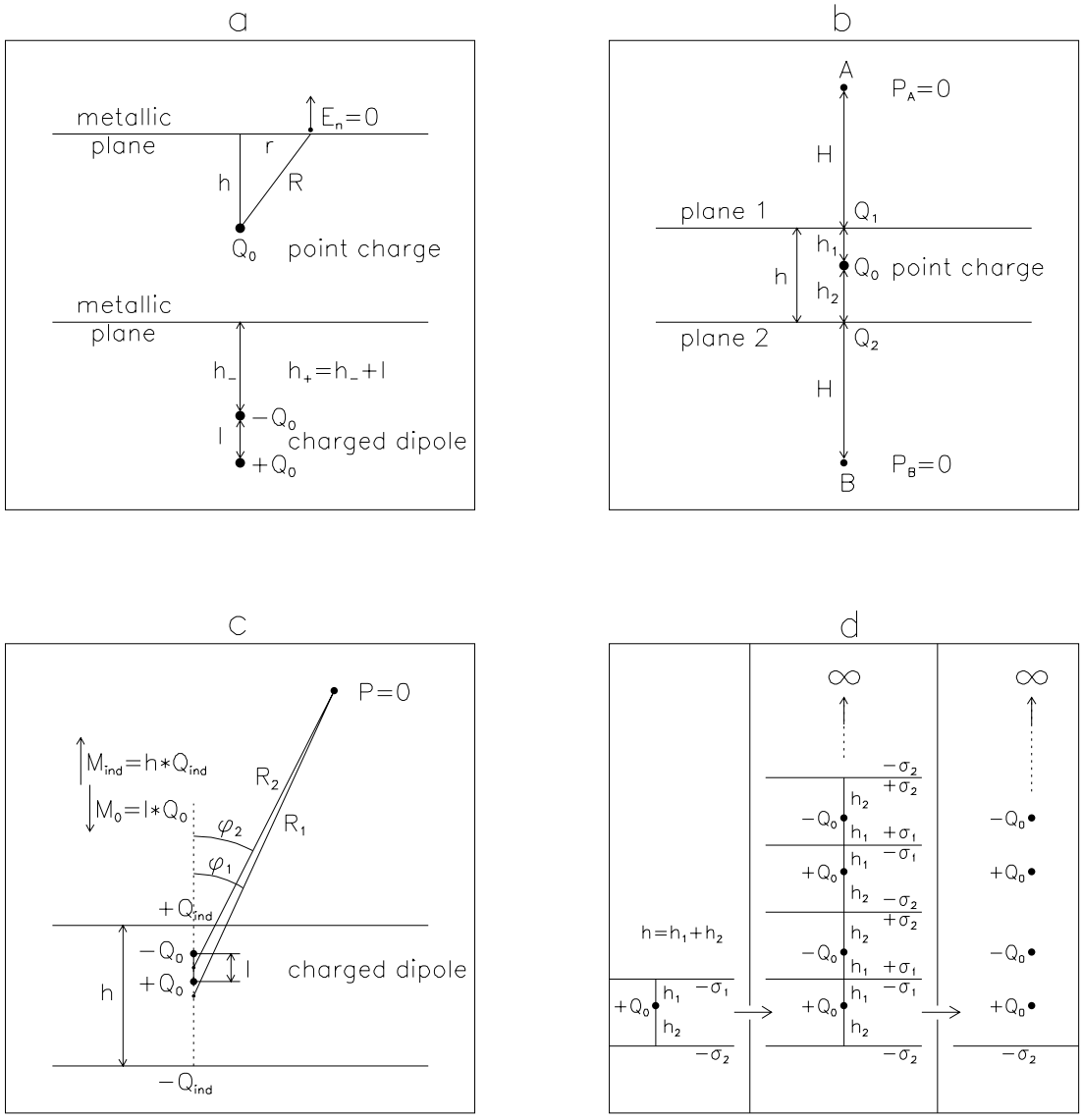


Fig. 1. Schemes for explanation of induced charge from point charge and charge dipole.

### 1.5. Induced charge density distribution from point charge and charged dipole for their position between two metallic planes

The method for the solving of this task is based on the consequent mirror reflection of the initial set of the charges and planes relative to one of the external planes (Fig.1d). This consequent reflection allows one to exclude a plane and the task becomes equivalent to that considered in Section 1.2.

Fig.1d shows, for example, how the initial task with the point charge between two planes (left part of the picture) transforms into the task for an infinite set of the point charges near one plane (right part of the picture).

According to Fig.1d and formula (4) the unknown charge density distribution $\sigma$(r) in the plane with a distance $h_p$ up to the point charge is

$$\sigma(r) = -\frac{Q_0}{2\pi} \cdot \sum_{k=0}^{\infty} \left(\frac{2hk + h_p}{(r^2 + (2hk + h_p)^2)^{\frac{3}{2}}} - \frac{2h(k+1) - h_p}{(r^2 + (2h(k+1) - h_p)^2)^{\frac{3}{2}}}\right). \tag{15}$$

For the upper plane $h_p$=$h_1$, for the lower plane $h_p$=$h_2$.

For an acceptable accuracy there is no necessity to realize an infinite sum. To provide the accuracy no worse, for example, than $\delta$, we can restrict the sum up to N, which is defined from the condition

$$\frac{r^2 + (2h - h_p)^2}{r^2 + (2h(N+1) - h_p)^2} \leq \delta^2 \tag{16}$$

and add to the sum an additional member

$$-\frac{Q_0}{2\pi} \cdot \frac{2h(N+1)}{(r^2 + 4h^2(N+1)^2)^{\frac{3}{2}}}, \tag{17}$$

which takes into account the influence of the last-mentioned unbalanced N plane, replaced by the equivalent point charge $Q_0$.

Thus, the following expression with the finite summarizing

$$\sigma(r) = -\frac{Q_0}{2\pi} \cdot \sum_{k=0}^{N} \left(\frac{2hk + h_p}{(r^2 + (2hk + h_p)^2)^{\frac{3}{2}}} - \frac{2h(k+1) - h_p}{(r^2 + (2h(k+1) - h_p)^2)^{\frac{3}{2}}}\right) - \\ -\frac{Q_0}{2\pi} \cdot \frac{2h(N+1)}{(r^2 + 4h^2(N+1)^2)^{\frac{3}{2}}} \tag{18}$$

allows one to get the required accuracy for the induced charge density distribution.

The correctness of mirror reflection method is confirmed, in particular, in the task: the long charged wire between two planes. Exact analytical solution [3] for the induced charge density distribution in the planes is

$$\sigma(r) = -\frac{\tau}{2h} \cdot \frac{sin(\pi \frac{h_p}{h})}{cosh(\pi \frac{r}{h}) - cos(\pi \frac{h_p}{h})}. \tag{19}$$

Here $\sigma$(r) is the surface charge density in the radial (transverse to the wire) direction, $\tau$ is the linear charge density of the wire, $h_p$ is a distance from the wire up to the plane, where we are interested in the induced charge density distribution.

According to the mirror reflection method, the induced charge density distribution from the wire is determined as:

$$\sigma(r) = -\frac{\tau}{\pi} \cdot \sum_{k=0}^{N} \left( \frac{2hk + h_p}{r^2 + (2hk + h_p)^2} - \frac{2h(k+1) - h_p}{r^2 + (2h(k+1) - h_p)^2} \right) - \\ - \frac{\tau}{\pi} \cdot \frac{2h(N+1)}{r^2 + 4h^2(N+1)^2}. \quad (20)$$

This expression with accuracy $\sim$0.01% agrees with analytical formula (19), when N is estimated from condition (16) with $\delta$=0.01.

To get the induced charge density distribution from M point charges $Q_i$ (and, in particular, from the charged dipole), we can again apply the superposition principle

$$\sigma(x,y) = -\sum_{i=1}^{M} \frac{Q_i}{2\pi} \cdot \left( \sum_{k=0}^{N} \left( \frac{2hk + h_i}{(r_i^2 + (2hk + h_i)^2)^{\frac{3}{2}}} - \frac{2h(k+1) - h_i}{(r_i^2 + (2h(k+1) - h_i)^2)^{\frac{3}{2}}} \right) \right) - \\ - \sum_{i=1}^{M} \frac{Q_i}{2\pi} \cdot \frac{2h(N+1)}{(r_i^2 + 4h^2(N+1)^2)^{\frac{3}{2}}}. \quad (21)$$

Here $r_i^2 = (x - x_i)^2 + (y - y_i)^2$ and $h_i$ is a distance from the charge $Q_i$ up to the plane with the induced charge density distribution in question. The value N is the same for all charges $Q_i$ and is defined from condition (16) and for the charge, which gives the maximal value N.

The method of mirror reflection doesn't allow one to get the induced charge density distribution in the presence of dielectric plates (actual RPC), because mirror reflection doesn't exclude the internal bakelite-gas surfaces with unknown distribution of polarized charge. Therefore, for an actual RPC we apply SCM calculation procedure, which is preliminary testified by comparison with the known analytical solutions.

In contrast to parallel external supplied field, the field from an avalanche (point type object) gives an unbalanced polarized charge in a flat dielectric. To keep zero balance for polarized charges, it was necessary to use additional equations in the calculational procedure

$$\int_S \sigma_p(s) ds = 0 \quad (22)$$

for each dielectric plate. Here $\sigma_p$(s) is the dielectric surface polarized charge density.

## 2. Comparison of SCM calculations with analytical predictions

First of all, the correctness of SCM calculation procedure was testified by classical task: linear capacitance(F/m) of two long parallel metallic rods (see Fig.2a). An analytical

expression for linear capacitance [4] is written in Fig.2a. We apply positive(+1V) potential to the left rod and keep the right rod under the ground potential. Then, we calculate by the SCM procedure the surface charge density distribution (Fig.2b), which provides these potentials for the rods. Calculations are made for three distances between the rods: 1 mm, 1 cm and 10 cm. Then, when we know the charge density distribution, we have a possibility to define the linear charge densities for both rods. And for the known potentials the linear capacitance is defined by the classical expression for the capacitance $C=0.5\cdot(\Delta Q/\Delta U)$. Here $\Delta Q$ is the algebraic difference between linear charge densities(C/m) of the left and right rods and $\Delta U$ is the respective algebraic difference between the potentials.

The dependence of calculated surface charge density on the azimuthal angle $\varphi$ for the left rod is presented in Fig.2b. The right rod repeats the charge density distribution of the left rod, but with less amplitude and with opposite sign. In Fig.2b we also write linear charge densities for both rods (left table) and compare the calculated ($C_{calc}$) linear capacitance with the exact analytical ($C_{an}$) solution (right table). As one can see, the agreement is good.

The left table in Fig.2b contains useful information. If we compare charge values of the rods for different distances between them, we find that, in absolute value, these charges will be equal to one another only at zero distance between the rods. Thus, the symmetry of free charges ($Q_1+Q_2=0$) for two objects under different potentials is possible either for the symmetry potentials ($U_1+U_2=0$) or for the arbitrary potentials but zero distance between objects. Polarized (in dielectric surface) charges every time have symmetry, because the total polarized charge of dielectric object is every time equal to zero. It explains, why the surface charge density for polarized charges is defined only by the potential difference and doesn't depend on the absolute value of the potentials, but surface charge density for free charges is defined by the values of supplied potentials. More simply: free charges "feel" both the potential and the potential gradient, polarized charges "feel" only the potential gradient.

In Fig.3a the negative point charge 50 pC is placed at a distance 2 mm from the metallic plane. The total induced charge value according to (3) is about 100% of initiating point charge. The numerical SCM calculation is in a good ($\sim$0.3%) agreement with analytical solution (2). The fact that the induced charge $Q_{ind}$ is somewhat less than initiating charge $Q_0$ is explained by the finite area of the metallic plane, which is realized in the calculation. The equality can be only for an infinite dimension of the plane.

For the negative point charge 50 pC, which is located between two strip planes at a distance $h_1=2$ mm from the upper plane and $h_2=4$ mm from the lower plane, the result of numerical SCM calculation is presented in Fig.3b. Variation of the point charge position between two planes shows that the induced charge values in the planes with the accuracy no worse than 3% correspond to (10). The shape of calculated distributions with accuracy no worse than 0.5% is in agreement with analytical expression (18).

For the charged dipole ($\ell=100$ $\mu$m, $Q_0=50$ pC), that is placed at a distance 2 mm from the metallic plane, the result of SCM calculation (Fig.3c) is in a good ($\sim$0.1%) agreement with analytical predictions (5) and (6). The total induced charge, as expected, is about zero. On a large scale, the induced charge density behaviour is shown in Fig.3c (tail).

Fig.3d shows the calculation of induced charge density distribution from 50 pC charged dipole, that is placed between two metallic planes at a distance 2 mm from the upper plane and 4 mm from the lower plane. Variation of the dipole position shows that the induced charge values in both the planes practically don't depend on the dipole position and for a vacuum approach ($\varepsilon$=1) can be estimated by expression (13) with $\ell = \frac{1}{\alpha}$. The shape of distributions for both planes with accuracy ~0.2% agrees with (21). On a large scale, the induced charge density distribution is shown in Fig.3d (tail).

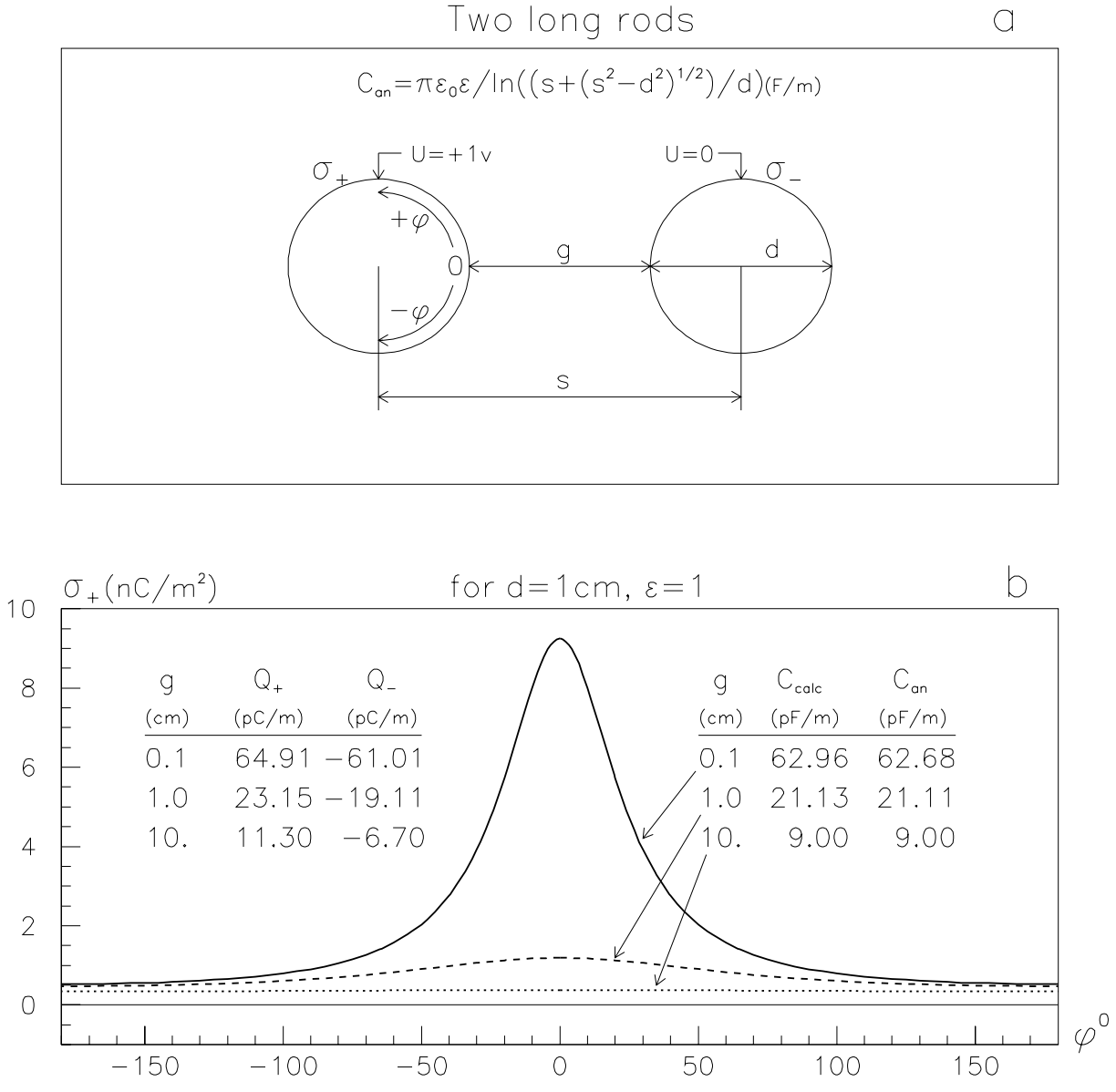


Fig. 2. Surface charge density distribution and capacitance for two long rods. Comparison SCM with analytical solution.

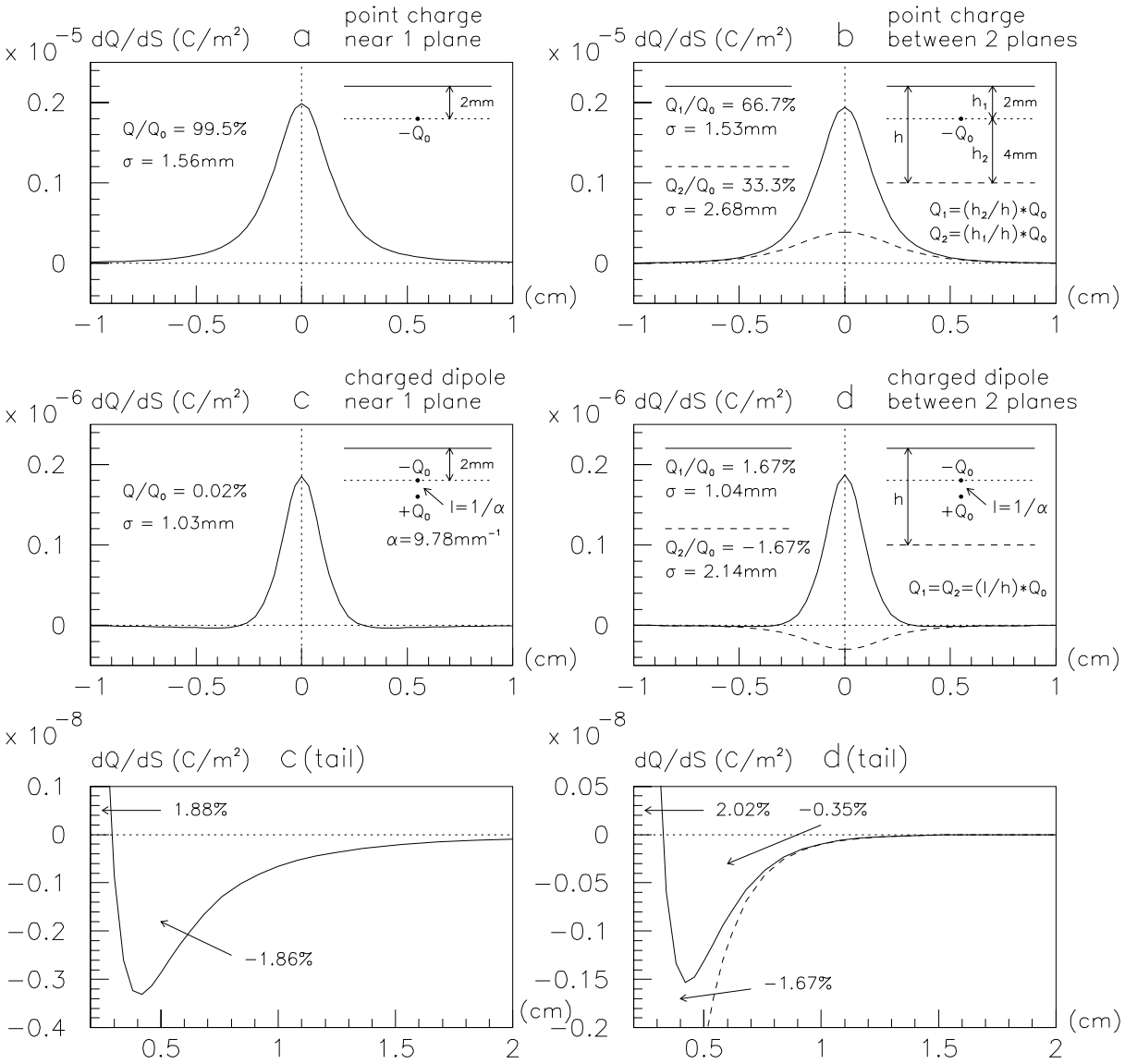


Fig. 3. Charge density induced from 50pC point charge and charged dipole.

An attempt to estimate the induced charge value by the well-known formula $Q_{ind} = \frac{1}{\alpha g} \cdot Q_0$, where g=2 mm is the gas gap value, gives 5.1%. This value is very far from being 1.67% (SCM calculation, Fig.3d) and from 1.7% (formula (13) with the distance between strip planes h=6 mm). Thus, for a vacuum approach ($\varepsilon$=1) estimation (13) is more correct. This estimation directly follows from (10) for induced charge from the two opposite sign point charges, which are combined in the charged dipole with an arm $\ell = \Delta h_1 = \Delta h_2 = \frac{1}{\alpha}$.

The dependences of the induced charge value both on electrode permittivity and thickness for 2 mm gap RPC are shown in Fig.4. Solid lines are for the induced charge in anode strip plane, dashed lines are for the induced charge in the cathode strip plane. We explain

the vertical shift between solid and dashed lines by asymmetric position of an avalanche relative to strip planes and finite transverse RPC dimension, which is realized in the calculations.

When the electrode thickness is reduced to zero, all the lines independently of the value of permittivity meet in one point. When the electrode thickness increases, the induced charge decreases down to zero. The value of induced charge grows with the increase of $\varepsilon$, but in the limit (infinite $\varepsilon$) has the plateau 4.8% for t=1 mm and 4.5% for t=5 mm, which is due to the full $\varepsilon$–conductivity of electrodes. For the actual RPC composition (2 mm gap and 2 mm electrodes), the value of induced charge varies from 1.7% at $\varepsilon$=1 up to 3.7% at $\varepsilon$=5.

All the dependences in Fig.4 with the accuracy no worse than 6% agree with (14).

The fact that the value of induced charge at the infinite $\varepsilon$ is not equal exactly to 5.1% according to (14) we explain by the finite transverse RPC dimension that is realized in the calculations.

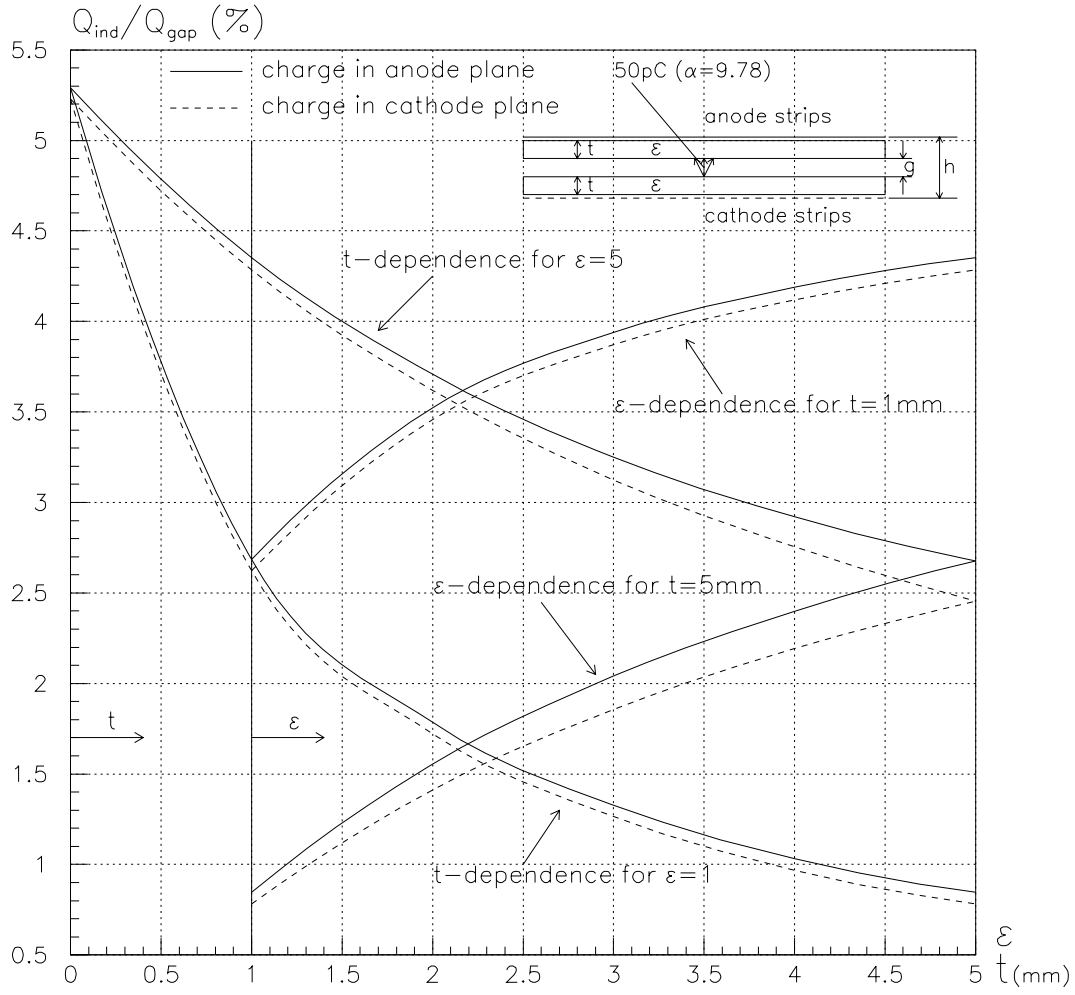


Fig. 4. Induced charge in dependence on electrode permittivity ($\varepsilon$) and thickness (t). Gap (g) is fixed 2mm.

## 3. Electric field in avalanche region

Fig.5 shows the distortion of 10 kV supplied field by the fast component of 50 pC avalanche in 2 mm gap RPC with 2 mm bakelite plates (permittivity $\varepsilon$=4). The SCM procedure takes into account the presence of both volume and surface currents. Volume and surface resistivities for bakelite and gas are taken from [1].

To make an avalanche charge distribution closer to the realistic one, we realized the following spacial avalanche configuration (see Fig.5a).

Negative avalanche head (labeled in Fig.5a by symbols "–") is presented as disk with the Gauss radial distribution of the charge

$$\frac{dQ}{dr} = \frac{Q_0}{\delta\sqrt{2\pi}} \cdot e^{-\frac{r^2}{2\delta^2}}. \tag{23}$$

Here $\delta$ is the dispersion of distribution, $Q_0$ is the total charge in the given disk.

The value of dispersion $\delta$ can be estimated from the assumption that in the first approximation the charged dipole from an avalanche (at the moment, when positive ions reach the cathode) can be presented as a round plate capacitance with gap g=2 mm and unknown radius $\delta$

$$C = \frac{1}{2} \cdot \frac{(Q_+ - Q_-)}{\Delta U} = \frac{|Q|}{|U|} = \frac{\varepsilon_0 S}{g} = \frac{\varepsilon_0 \pi \delta^2}{g}. \tag{24}$$

From formula (24) for 50 pC avalanche and 10 kV voltage, we get $\delta$=0.6 mm. The same estimation follows from the conception of saturated charge density, which requires for any discharge process the transported charge density of electrons to be not higher than the surface charge density of free charges (44 pC/mm$^2$), which is provided by 10 kV voltage at bakelite-gas boundary. Let the electrons transported by an avalanche head to the anode, be presented simply as the negative disk with the constant charge density. Then, according to the conception of saturated charge density for 50 pC avalanche, we write

$$\frac{50pC}{\pi\delta^2} = 44\frac{pC}{mm^2} \tag{25}$$

and again $\delta$=0.6 mm.

Positive ions (labeled in Fig.5a by symbols "+") are presented as four separate disks also with the Gauss radial distribution of the charge. Ions multiplicity in each positive disk varies exponentially in the direction of avalanche motion. Dispersion for the Gauss charge distribution in each disk has linear variation from minimal value 0.12 mm for the first positive disk up to 0.6 mm for the last negative disk. The radius of each charged disk in Fig.5a is shown as one standard deviation for the Gauss charge distribution in the given disk. Position of each positive disk is defined from the coordinate averaging with exponential probability function. Thus, in 2 mm gap in the direction of an avalanche motion the coordinates of positive disks are 0.4, 0.9, 1.4 and 1.9 mm. The negative disk has coordinate 2 mm. The positive disks contain (respectively to exponential discharge process) the following charge values: $2{\cdot}10^{-5}$, $3{\cdot}10^{-3}$, 0.37 and 49.6 pC.

Fig.5a shows the field behaviour in the region of 50 pC avalanche. We see that in the RPC gap electric strength lines are practically parallel as before. Variation is present only for the absolute field value.

Potentials at different levels in the gas gap are shown in Fig.5b. Along the upper bakelite-gas surface in the transverse direction at a distance $\sim$ 1 mm from an avalanche axis the field is sufficiently (96%) close to the operating voltage. In the vertical direction at a distance $\sim$ 0.5 mm from the upper bakelite-gas surface, the field is also (96%) close to plateau voltage value for the given level.

Thus, the region, where the field drop is higher than 4% in comparison with the operating voltage, in the horizontal direction is about 2 mm, in the vertical direction near the anode plate is about 0.5 mm. Note once again, that the estimations above were made for the fast component of the exponential discharge process.

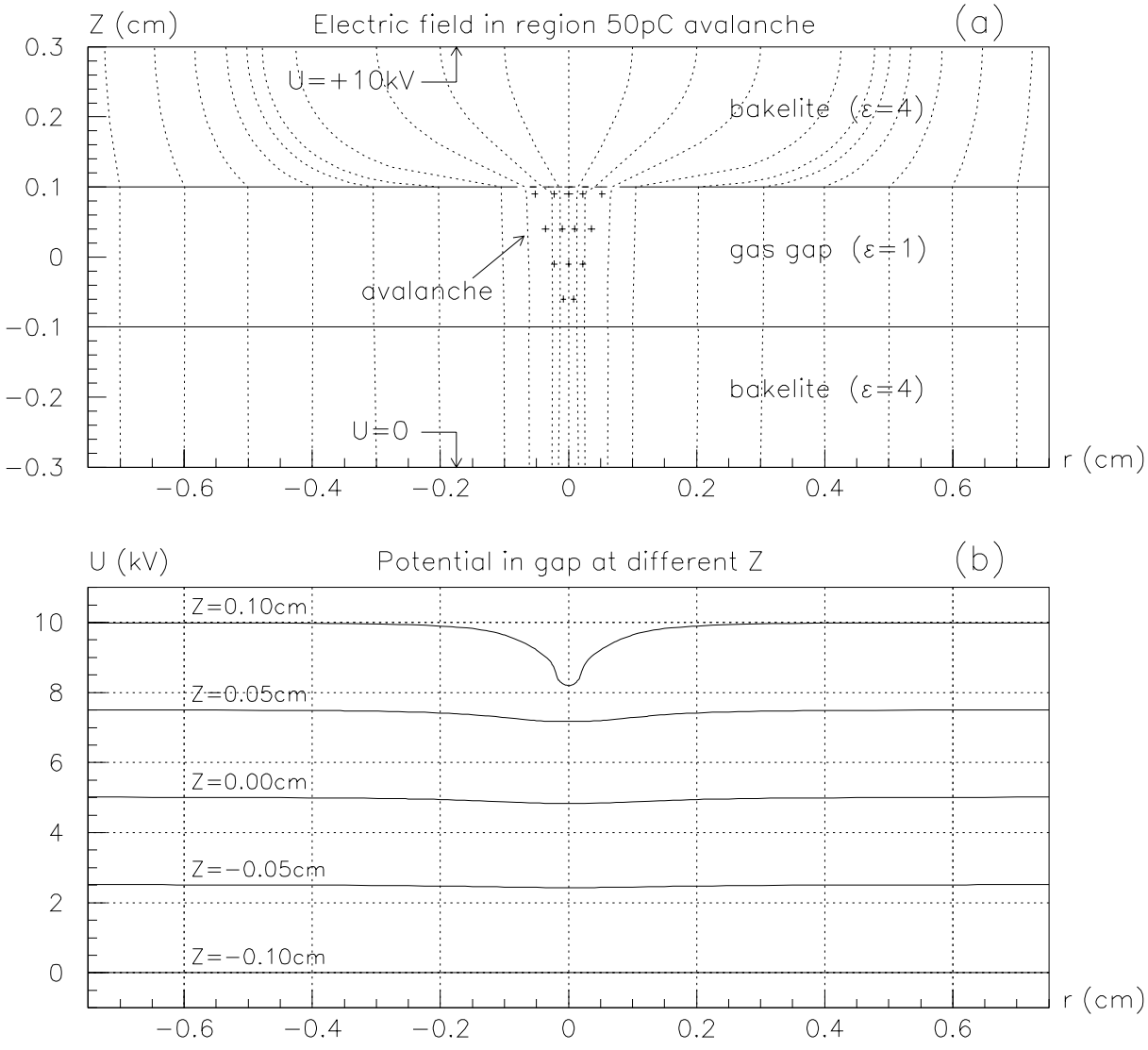


Fig. 5. Distortion of 10kV supplied field by 50pC avalanche.

# 4. Influence of gap in foil coating and external ground plane on the value of induced charge

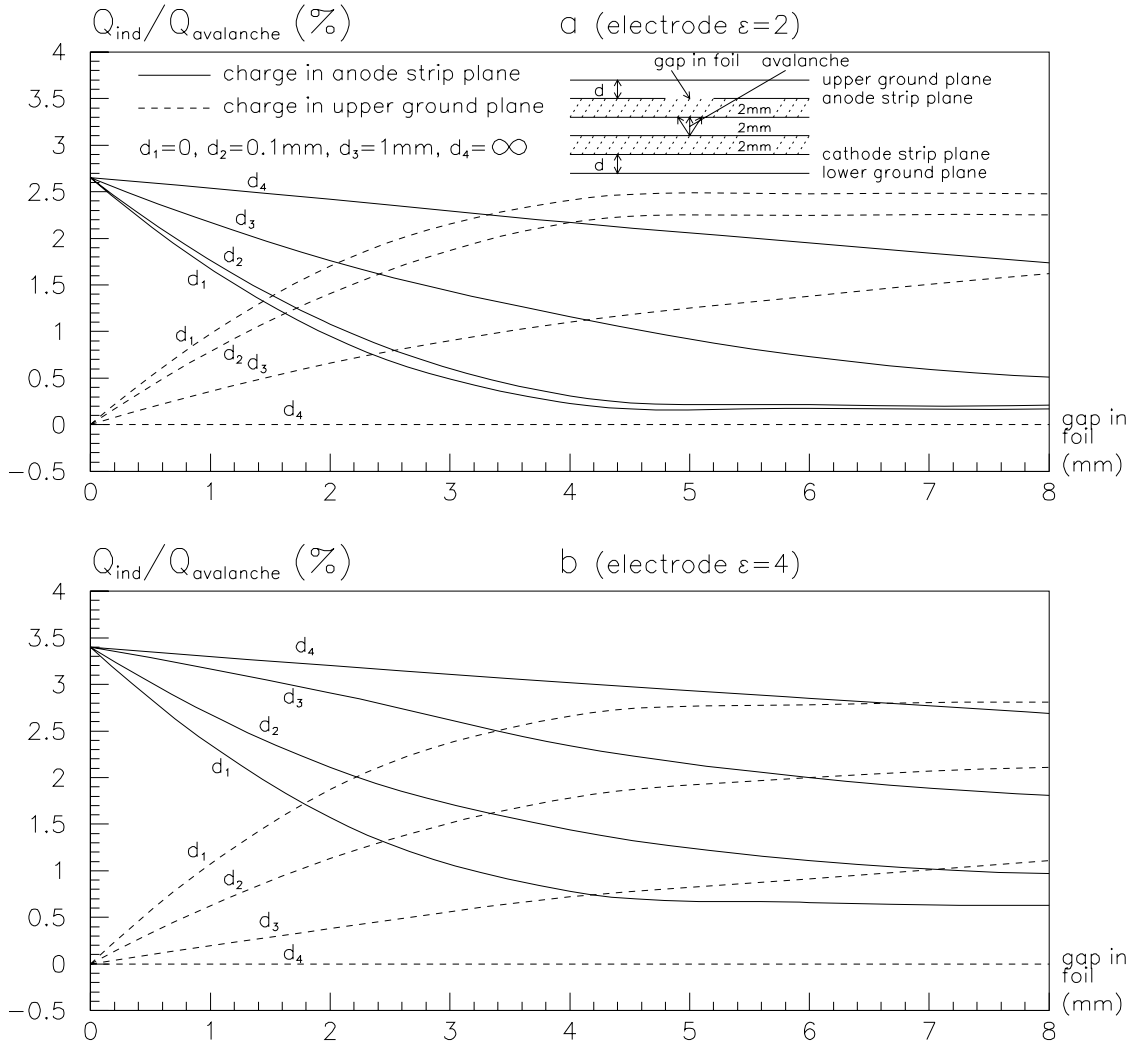


Fig. 6. Induced charge as function of gap in foil and distance between ground and strip planes.

The next step was to understand the influence of foil-uncoated region and additional external ground planes on the value of induced charge.

For this purpose we varied the value of uncoated with foil gap in anode strip plane and the distance between ground and strip plane (see scheme in Fig.6a). The maximal influence of the ground plane on the value of induced charge in the anode plane is expected, when the particle goes through the gap in foil coating. Therefore, the avalanche was placed exactly against the centre of the gap in foil coating (see Fig.6a). Electrode thickness (2 mm) and gas gap (2 mm) were fixed. Calculations were made for two electrode permittivities: $\varepsilon$=2 (Fig.6a) and $\varepsilon$=4 (Fig.6b). Ground planes were separated from strip planes by the matter with $\varepsilon$=1.

Solid lines in Fig.6 show the induced charge in the anode plane, dashed lines show the induced charge in the ground plane, that is nearest to anode. In the ground plane, that is nearest to cathode, the induced charge value for this scheme is every time practically zero. In the cathode strip plane the induced charge has the opposite sign and in the absolute value is practically equal to the total charge, that is induced in the anode strip and ground planes.

As expected, the value of induced charge in the anode strip plane falls and in the nearest ground plane grows, when the gap in foil increases and the distance between ground and strip plane decreases.

If we compare the dependences in Fig.6a and Fig.6b, we'll find that the influence of the ground plane is higher, when the electrode permittivity is less.

## 5. Charges induced in read-out strips. Static solution

### 5.1. Unbroken foil coating

For $50\times50$ cm$^2$ RPC with 2 mm gas gap and electrode thickness 2 mm the dependence of induced charge in the pick-up and in the neighbouring read-out strip on an avalanche position for an unbroken foil coating was calculated for two electrode permittivities. The former (Fig.7) for $\varepsilon$=1, the latter (Fig.8) for $\varepsilon$=4. It was specially done to demonstrate that the different electrode permittivities give the different values of induced charges in anode and cathode strips (compare Fig.7 and Fig.8). Pick-up read-out strip in the pictures is labeled as 1, neighbouring read-out strip is labeled as 2. For the anode plane the value of induced charge in strip is normalized on the positive value of an avalanche charge. For the cathode plane the normalization is made on the negative value of an avalanche charge.

Tiny strips provide the unbroken foil coating, but have no direct contact with read-out strips. Overall period (tiny strip width + read-out strip width) is the constant 30 mm value. The tiny strip width varies from 0 up to 8 mm, read-out strip width varies from 30 mm down 22 mm, respectively.

It is necessary to point that the induced charges in the anode and cathode read-out strips in Figs. have no direct correlation at the given avalanche position. The dependences are simply presented in Figs. with the same coordinate scale to show the difference of the induced charge values and to compare the behaviour of the induced charges in anode and cathode read-out strips. If we call neighbouring read-out strip 2 as the right neighbouring one, then the dependence of induced charge in the left neighbouring strip can be obtained by simple mirror reflection (Y-coordinate) of the dependence for the right neighbouring strip relative to the central point of pick-up strip 1.

When an avalanche position varies along Y direction during one period (30 mm), the value of induced charges in read-out strips 1 and 2 also varies. These variations are shown in Figs. by solid lines for read-out strips 1 and 2 in anode strip plane and by dashed lines for read-out strips 1 and 2 in cathode strip plane. A vertical dotted line shows the mathematical boundary between the tiny and read-out strip. The value of induced charge in a whole strip plane is shown by a horizontal thick line.

The main reason of Fig.7 (vacuum solution) is to demonstrate a very important role of electrode permittivity and below we are discussing only Fig.8.

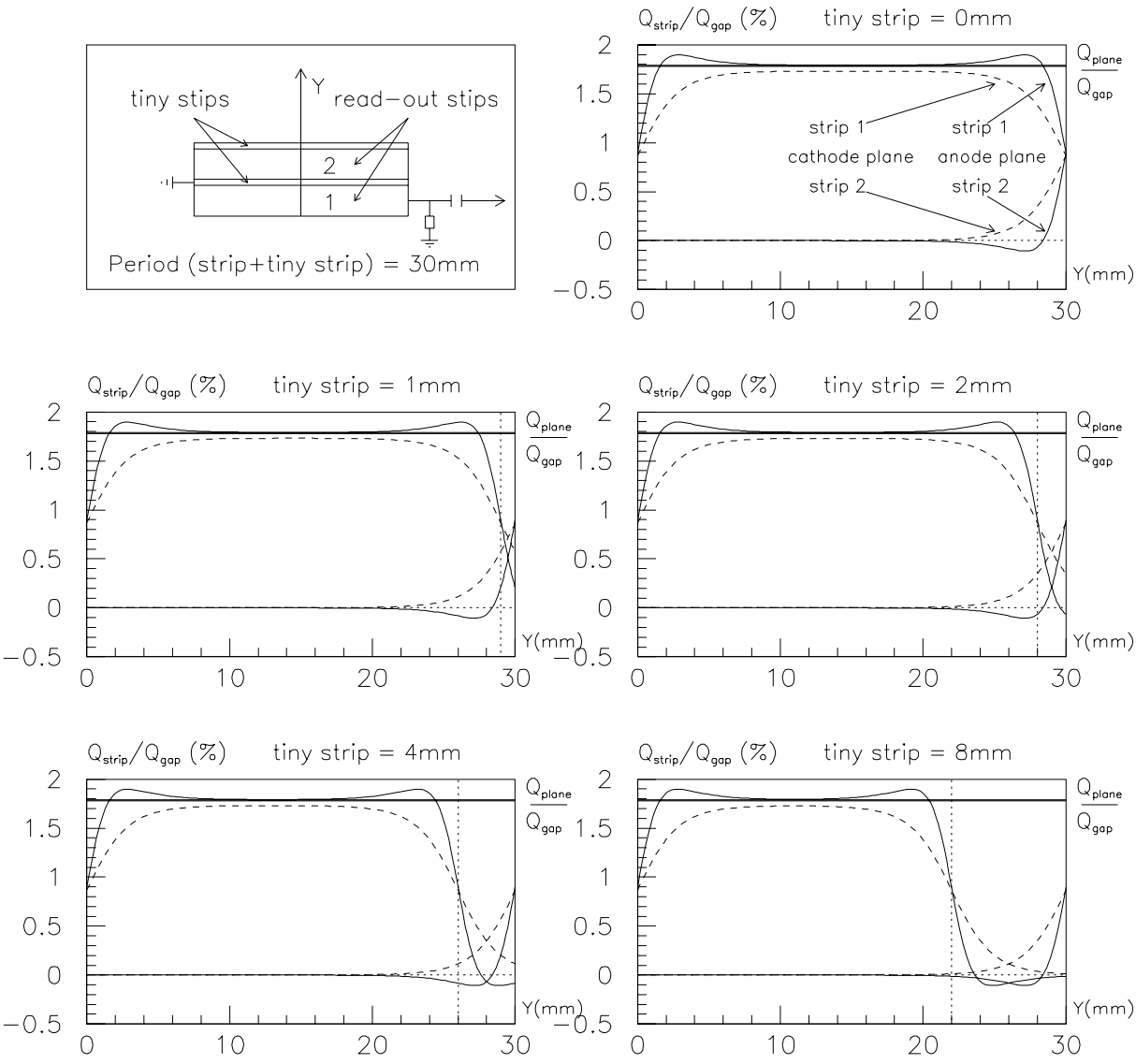


Fig. 7. Read–out strip charges in dependence on avalanche position. Unbroken foil coating. Electrode $\varepsilon$=1.

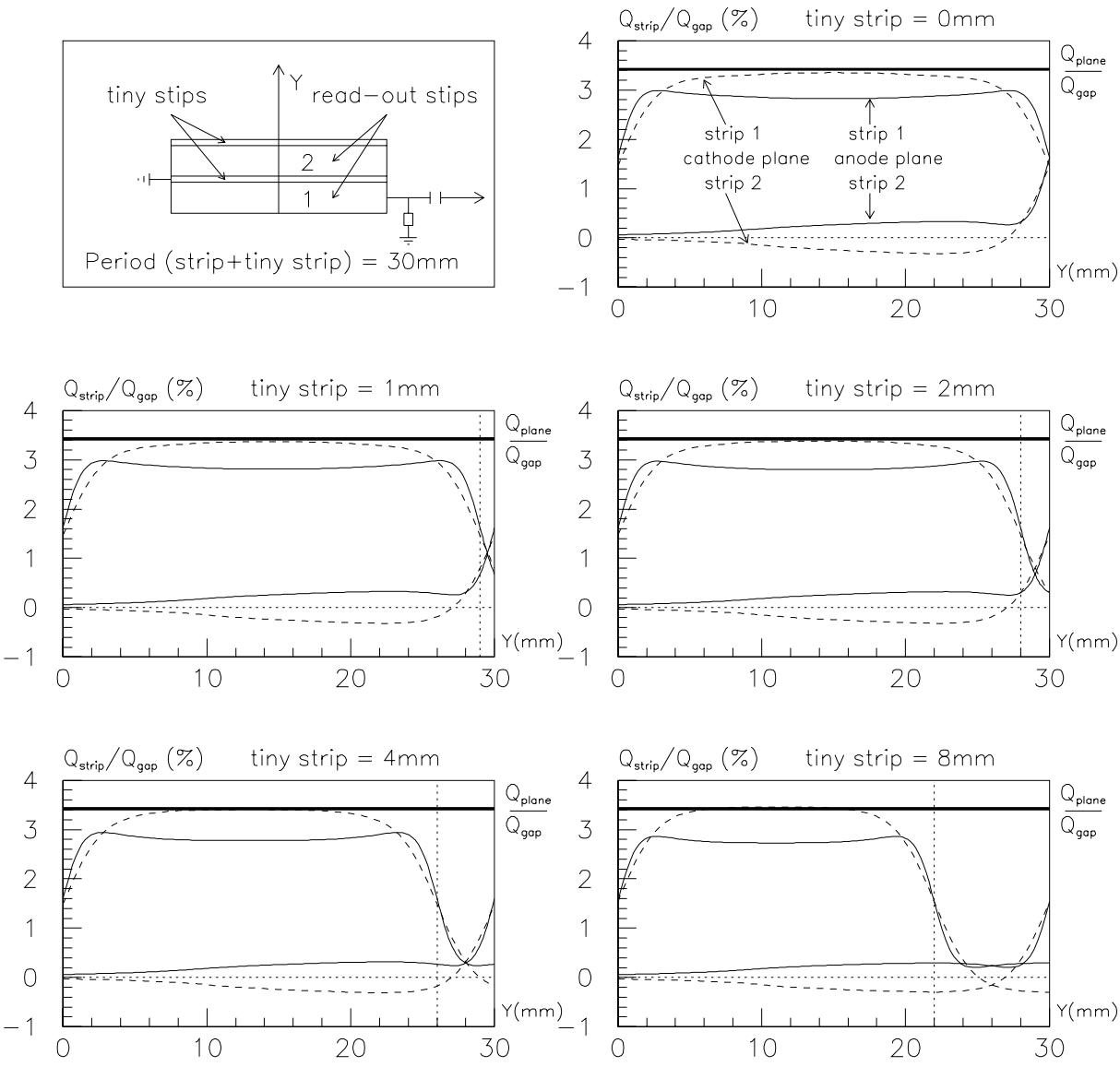


Fig. 8. Read–out strip charges in dependence on avalanche position. Unbroken foil coating. Electrode $\varepsilon$=4.

When an avalanche position is against the pick-up strip, most of the total induced charge is concentrated in pick-up strip both for anode and for cathode plane. For uniform particles flux, the average induced charge in anode pick-up strip is about 90% in comparison with average induced charge in cathode pick-up strip. The relation of average induced charge in the neighbouring strip to average induced charge in pick-up strip for anode plane is about 9%, for cathode plane is about 7%. In addition, for cathode plane the induced charge in the neighbouring strip has an opposite sign versus the charge sign in the pick-up strip.

It is necessary to note that in contrast to the total induced charge, when the anode plane has somewhat higher value of induced charge in comparison with the cathode plane (see Fig.4), an anode pick-up strip has a lower value of induced charge in comparison with the cathode pick-up strip. The explanation to this feature is as follows: For each particular RPC (gas gap, electrode thickness and permittivity) the induced charge density distribution in a whole strip plane has varying with radius (varying amplitude, dispersion and sign) shape. The induced charge value in each strip is defined by the integral over the strip area, that overlaps with a particular fragment of the total charge density distribution. Therefore, the dependence on the given parameter for the induced charge in a separate strip does not follow obligatorily the dependence for the induced charge in a whole plane.

The induced charge value in the pick-up strip falls quickly, when an avalanche position shifts to the region of the tiny strip. For the tiny strip width, that is equal or higher than 2 mm, the signal from the particle passing through the tiny strip is small.

### 5.2. Broken foil coating

Fig.9 shows the value of induced charges in read-out strips for the broken foil coating. Horizontal thick lines show the value of induced charge in a whole plane for the unbroken foil coating.

The relation between average induced charges in anode and cathode pick-up strips and the relation between average induced charges in the neighbouring and pick-up strip are approximately the same as for the unbroken foil coating. In comparison with the unbroken foil coating, we here observe a more significant induced charge from the particles that pass through the gap between read-out strips.

If we add external ground planes, we get the result, that is median between the results of Section 5.1 and 5.2, because the unbroken foil coating is equivalent to zero distance between external ground planes and strip planes and the broken foil coating is equivalent to infinite distance.

The main conclusion that follows from Sections 4, 5.1 and 5.2 is the following: The maximal efficiency for particles detection is reached for the narrow gap between strips both for broken and unbroken foil coating.

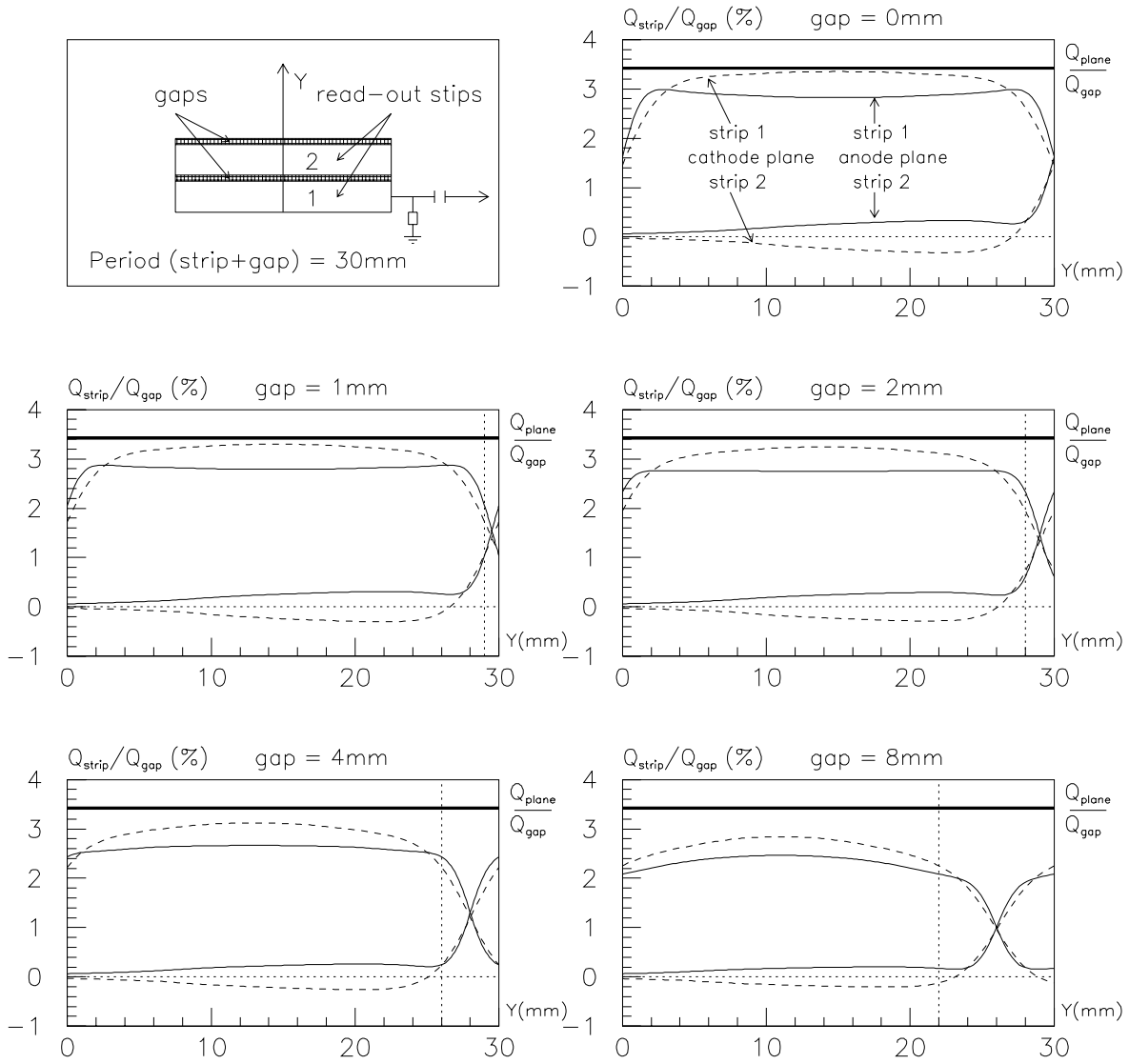


Fig. 9. Read–out strip charges in dependence on avalanche position. Broken foil coating. Electrode $\varepsilon$=4.

### 5.3. Different strip widths

Fig.10 shows the induced charge in read-out strips versus an avalanche position for different strip widths and for unbroken foil coating. The tiny strip has zero width.

This Fig. shows that for the chosen RPC composition (gas gap 2 mm, electrode thickness 2 mm and electrode permittivity $\varepsilon$=4) the minimal strip width must be about 40 mm. This width, on the one side, provides practically the same induced charge in anode and cathode pick-up strips, on the another side, the value of induced charge in pick-up strip in both the planes is practically plateau, when an avalanche position varies from the left strip edge to the right strip edge. Hence, this minimal strip width provides a sufficient efficiency for particles detection.

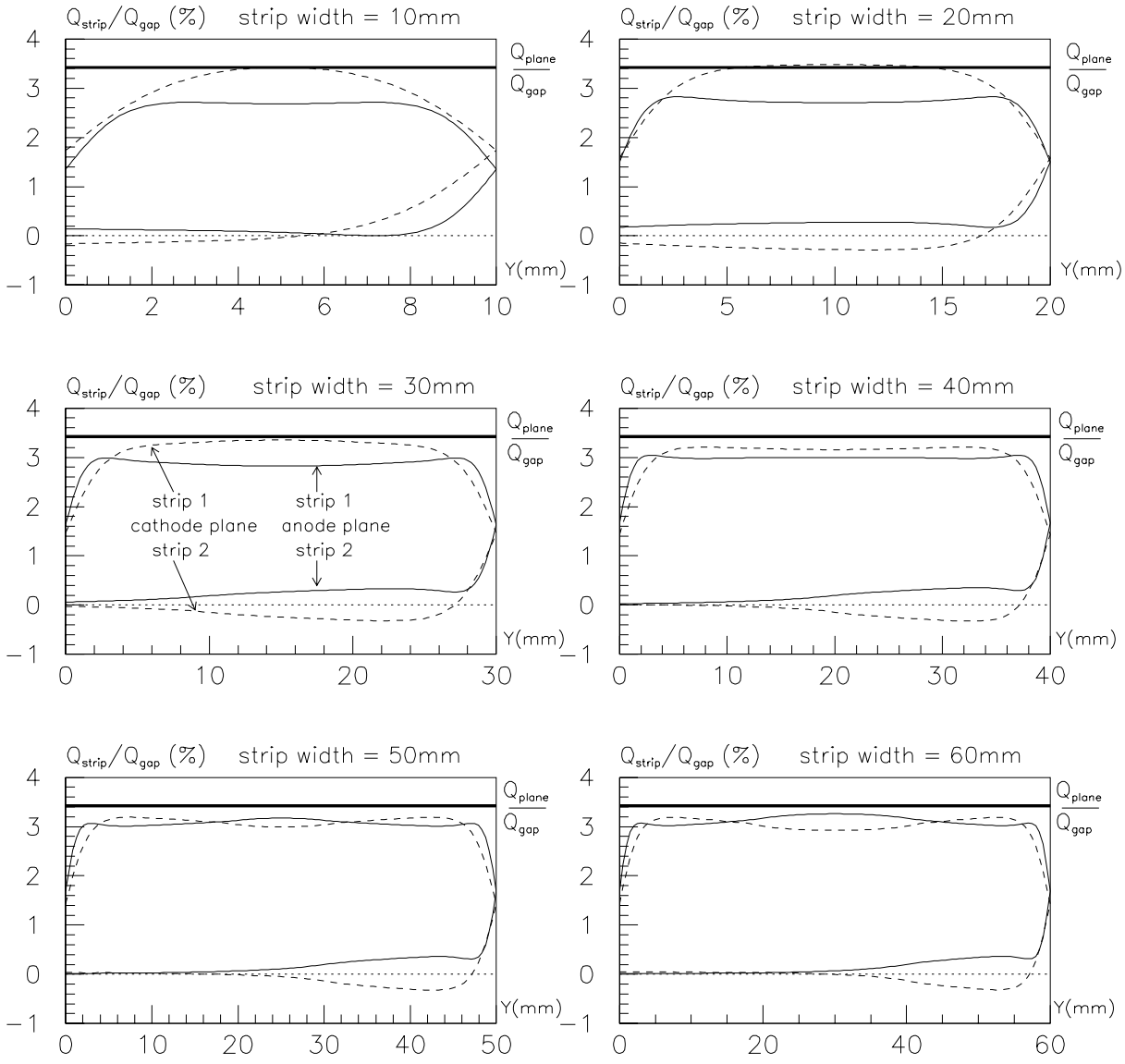


Fig. 10. Read–out strip charges in dependence on avalanche position for different strip width. Electrode $\varepsilon$=4.

## 6. Voltage signals. Dynamic solution

For the calculation of voltage signal in the separate strip, we apply two additional conditions, which characterize a quick dynamic process.

The first condition is the law of charge conservation during the signal spread along the strip. It means that during the time

$$\Delta t = \sqrt{\varepsilon} \cdot \frac{\ell}{c} \tag{26}$$

(here $\varepsilon$ is the electrode permittivity, c is the light velocity, $\ell$ is the signal way in the strip) the total free charge in the given strip is the constant value, that was before the discharge process. And the following condition for every strip

$$\int\limits_S \sigma_f(s)ds = Q_{fixed} \tag{27}$$

(here $\sigma_f$(s) is the surface free charge density) is added to the system of equations that are used for field calculation in [1].

The induced charge density in the pick-up region is varying in time value and to provide the law of charge conservation (27) in the quick dynamic process, an additional (second) condition is applied: Running along the strip the potential waves and, respectively, charge clusters. From a physical point of view, it means that all the strip surface, excluding the region of running wave, has the potential that was before the discharge process. Since we don't initiate a potential in the region of running waves, we lose part of equations, but to keep equality between the number of equations and unknowns, we add equations (27).

Because the length of running wave is defined by the discharge process time, it is necessary to get an estimate for the wave length to apply in calculations.

According to [2], the total charge in the gap as function of time is determined by the expression:

$$Q(t) = en(g - vt)e^{\alpha vt} + env\int\limits_0^t e^{\alpha v\tau}d\tau = en(g - vt)e^{\alpha vt} + \frac{en}{\alpha}(e^{\alpha vt} - 1). \tag{28}$$

Here e is the electron charge, n is the average density of primary electrons along the track, g is the gap value, v is the drift velocity, $\alpha$ is the Tounsend coefficient.

Applying formula (14), we estimate the induced charge value

$$q(t) = \frac{en}{\alpha(g + 2\frac{d}{\varepsilon})} \cdot ((g - vt)e^{\alpha vt} + \frac{1}{\alpha}(e^{\alpha vt} - 1)). \tag{29}$$

Here d is the electrode thickness. Then, we take the first derivative over the time and determine as in [2] an induced current in the strip

$$i(t) = \frac{env}{g + 2\frac{d}{\varepsilon}}(g - vt)e^{\alpha vt}. \tag{30}$$

Fig.11a shows the behaviour in time of induced current and induced charge for the following parameters: n=5 mm$^{-1}$, gap is 2 mm, the time of the quick discharge process is 20 nsec (v=0.1 mm/nsec), $\alpha$=9.78 mm$^{-1}$.

We see that the time wave length of the current signal is about 3 nsec for 20 nsec process. The $\Delta$t interval shown by arrows in Fig.11a, consists of two standard deviations the for current signal distribution.

We take, for simplicity, the 30 cm cluster length. For electrode permittivity $\varepsilon$=5, this length is equivalent to $\Delta t = \sqrt{\varepsilon}\cdot(\ell/c)$=2.25 nsec time wave length, that is of the same order as the estimated above.

Fig.11b shows the surface charge density and potential distributions in the anode strip at a moment, when the running waves pass half the way along the strip. Because of the large difference in charge densities in the pick-up and cluster region, we apply the logarithmic function of charge density to a vertical scale. The vertical scale for the potential distribution is in arbitrary units. We write only the amplitude value for the potential difference in the region of cluster.

The result of Fig.11b is calculated for the following RPC parameters: avalanche 50 pC, gap 2 mm, electrode thickness 2 mm, permittivity $\varepsilon$=5, distance between ground and strip plane 3 mm, permittivity for the material between ground and strip plane $\varepsilon$=1. For charge density distribution, we couldn't apply satisfactory spline procedure and points in the plot are simply connected by straight lines.

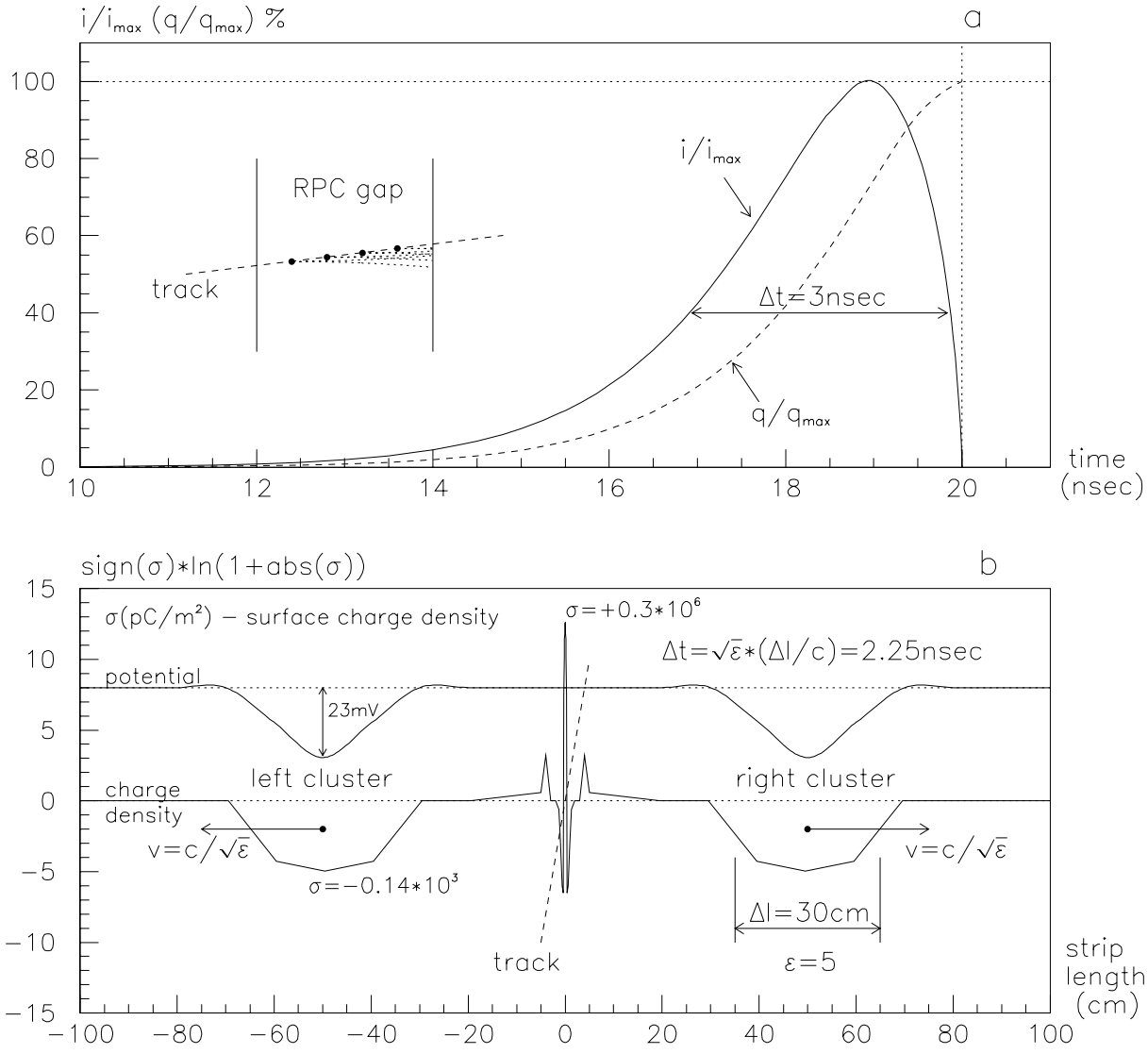


Fig. 11. Induced current and charge as function of time (a). Running potential waves and charge clusters in anode strip (b).

The dependences of voltage signal on electrode thickness, permittivity and distance between ground and strip plane are presented in Fig.12.

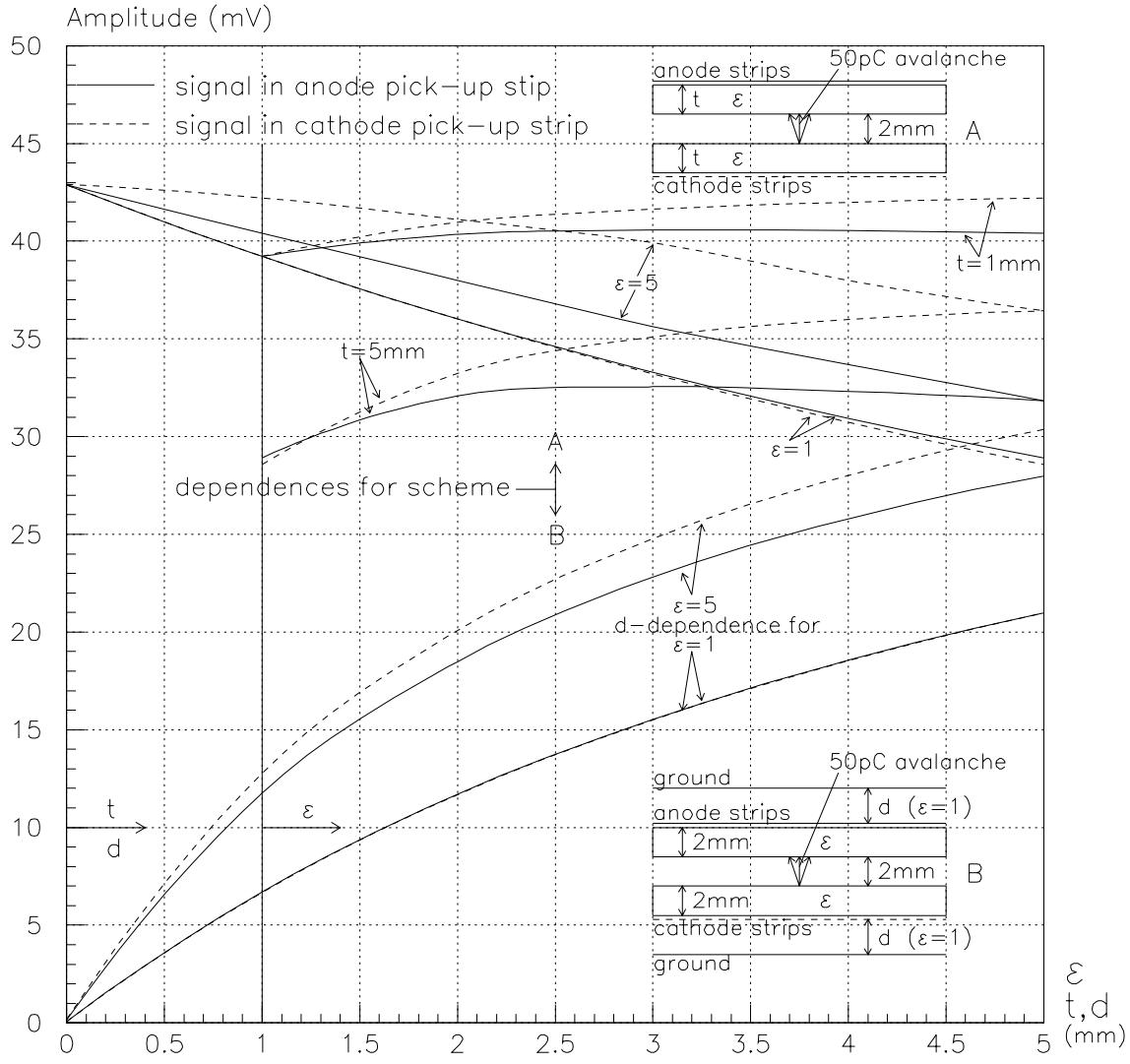


Fig. 12. Voltage signal in dependence on electrode thickness (t), permittivity ($\varepsilon$) and distance (d) between strip and ground planes.

If we compare the upper dependences (for scheme A) with the analogous dependences for induced charges (see Fig.4), we'll find a qualitative agreement between them. Both the induced charge and voltage signal grow with permittivity and fall, when electrode thickness increases. If we look at induced charges in pick-up strips (see Fig.8 and Fig.9), we find that the induced charge in cathode pick-up strip is higher in comparison with the induced charge in anode pick-up strip. The same result we have and for voltage signals (Fig.12). For $\varepsilon$=1, we have the contrary relation: Voltage signal in the cathode strip is somewhat less in comparison with voltage signal in the anode strip. But the same result we have and for the induced charges (see Fig.7). Thus, for the scheme without ground

planes, the voltage signal and induced charge in pick-up strips have a similar behaviour relative to the variation of electrode thickness and permittivity.

When we add ground planes (Fig.12, scheme B), a definite part of electromagnetic energy goes to form a running wave in the ground plane to provide zero potential after the ground plane. Therefore, the voltage signal in the strip plane is less and falls with the decrease of distance between the ground and strip plane.

A different result for static and dynamic solution we have for the neighbouring strip in the cathode plane. Static solution for $\varepsilon>1$ (Figs.8,9,10) gives a negative sign of induced charge in the neighbouring strip over the charge sign in the pick-up strip. Dynamic solution (Table.1, first line) gives the same sign of voltage signal both in the pick-up and in the neighbouring strip. A possible explanation is that with static solution the charge density distribution is defined mostly by an avalanche, but with dynamic solution, when the running clusters are sufficiently far from an avalanche, the values of charges in the clusters depend essentially on strip-strip capacitance coupling.

In Table 1 the voltage signals in the pick-up (left-hand values) and in the neighbouring (right-hand values) strips for anode and cathode planes versus the distance between the ground and strip plane are given for scheme B in Fig.12 with electrode permittivity $\varepsilon$=5.

**Table 1.** Voltage signals in anode and cathode strips.

| Distance between strip and ground plane | Signals in anode strips (mV) | Signals in cathode strips (mV) |
|---|---|---|
| d=$\infty$ | –38.00/–3.50 | +41.11/+2.64 |
| d=5mm | –27.97/–0.92 | +30.36/+0.17 |
| d=3mm | –22.82/–0.61 | +24.78/–0.01 |
| d=1mm | -11.75/–0.23 | +12.77/–0.09 |

We see that the decrease of distance between the ground and strip plane gives a more quick fall in voltage signal of the neighbouring strip in comparison with the respective fall in the pick-up strip.

For the same RPC scheme, the values of charges in the clusters (total charge of the left and right cluster) are given in Table 2. For the finite distances, we present two sets of the charges. The upper set is for the charges of clusters in the strips, the lower set is for the charges of respective clusters in the ground planes.

For the central track position relative to the pick-up strip axis, the value of induced charge in the pick-up strip doesn't practically depend on the distance between ground and strip plane (see Table 2) and can be estimated by expression (14). Every running charge cluster contains half the induced charge in the given strip.

According to Table 1 data, the voltage signal decreases with the distance between the ground and strip plane. According to Table 2 data, this falling is due to the growth (in the nearest ground plane) of the cluster with the opposite charge sign. In the limit (very

small distance between ground and strip plane) we have two closely running clusters with equal charge but of the opposite sign, and their total potential is respectively equal to zero.

**Table 2.** Charges of clusters in anode, cathode strips and ground planes.

| Distance between strip and ground plane | Clusters in anode strips and ground plane (pC) | Clusters in cathode strips and ground plane (pC) |
|---|---|---|
| d=$\infty$ | –1.71/–0.07 | +1.86/–0.03 |
| d=5mm | –1.71/–0.05<br>+0.58/+0.06 | +1.86/–0.04<br>–0.63/–0.03 |
| d=3mm | –1.71/–0.05<br>+0.80/+0.05 | +1.86/–0.04<br>–0.86/–0.01 |
| d=1mm | –1.71/–0.05<br>+1.24/+0.05 | +1.86/–0.04<br>–1.35/+0.01 |

For a while, we have no possibility to realize in dynamics the correct simulation of the task: The influence of a tiny strip on voltage signals in the strips. But it is clear that the tiny strip as well as the ground plane, on the one side, absorbs part of the voltage signal from the pick-up strip, on the other side, works as a screen between the pick-up and neighbouring strip and, respectively, decreases a signal in the neighbouring strip. The screening effect from the tiny strip is confirmed in the static task: Charge density distribution due to capacitance coupling (see Fig.13). Here the pick-up strip in the anode plane has the constant (positive potential), all other objects are under the ground potential. One set of numbers corresponds to the variant without tiny strips, another set of numbers (in brackets) corresponds to the variant with tiny strips. We see that the value of charge in the neighbouring strip falls approximately twice if we add 300 $\mu$m tiny strip.

## Conclusion

1. The region with field drop higher than 4% of the plateau field, that arises in 2 mm gap RPC under the action of an avalanche fast component, is about 2 mm in the transverse direction and is about 0.5 mm in the vertical direction near the anode plate.

2. The value of induced charge and voltage signal grows with electrode permittivity and falls, when the electrode thickness increases.

3. The external ground planes absorb a noticeable part of the total induced charge, when the particle passes through the gap between read-out strips and when the distance between ground and strip planes is small.

4. The maximal efficiency for particles detection is reached for the narrow gap between read-out strips for both broken and unbroken foil coating.

5. The decrease of distance between ground and strip planes gives quicker fall in the voltage signal of the neighbouring strip in comparison with the respective fall in the pick-up strip.

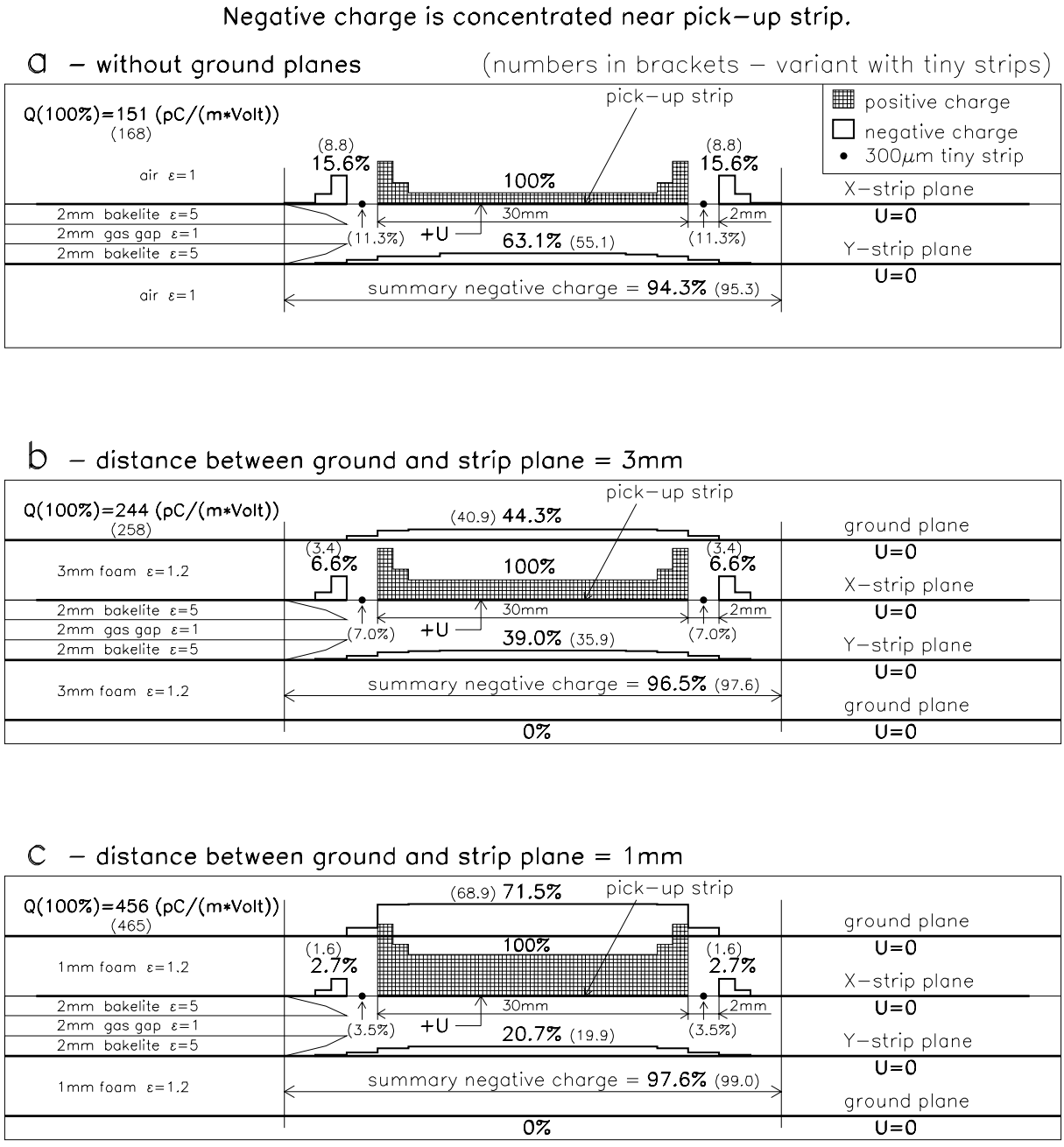


Fig. 13. Charge density distribution due to capacitance coupling. Charge density in arbitrary scale.

## References

[1] V.Ammosov, V.Korablev, V.Zaets, Electric field and currents in resistive plate chambers, Nucl. Instr. and Meth. A 401 (1997) 217.

[2] R.Santonico, Topics in resistive plate chambers, III Int. Workshop on Resistive Plate Chambers and related detectors, Scientifica Acta quaderni del dottorato. Vol.11, Anno 11, Num.1, 1996.

[3] E.Mathieson, Induced charge distributions in proportional detectors, Monograph, 1991, Leicester University, England.

[4] Theoretical Principles of Electrotechnics, Moscow: High School 2 (1976) p.170, (in Russian).

*Received November 25, 1997*

В. Аммосов, В. Кораблев, Р. Сантонико.
Наведенные заряды и импульсы напряжения в резистивных плоскопараллельных камерах.

Оригинал-макет подготовлен с помощью системы LaTeX.
Редактор Е.Н.Горина. Технический редактор Н.В.Орлова.

Подписано к печати 26.11.97. Формат 60 × 84/8. Офсетная печать.
Печ.л. 3,25. Уч.-изд.л. 2,29. Тираж 180. Заказ 132. Индекс 3649.
ЛР №020498 17.04.97.

ГНЦ РФ Институт физики высоких энергий
142284, Протвино Московской обл.

Индекс 3649

П Р Е П Р И Н Т 97-83, И Ф В Э, 1997